

1                                    **AN INTEGRATED APPROACH FOR THE PLANNING**  
2                                    **OF DREDGING OPERATIONS IN ESTUARIES**

3                                    M. Álvarez <sup>a</sup>, R. Carballo <sup>a\*</sup>, V. Ramos <sup>a</sup>, G. Iglesias <sup>b</sup>

4        <sup>a</sup> Univ. of Santiago de Compostela, Hydraulic Eng, EPS, Campus Univ. s/n, 27002  
5        Lugo, Spain

6        <sup>b</sup> Univ. of Plymouth, School of Marine Science and Engineering, Marine Building,  
7        Drakes Circus, Plymouth PL4 8AA, United Kingdom

8        **ABSTRACT**

9        Ports are often located in naturally sheltered areas such as estuaries. The strong tidal  
10        currents that occur in many of these areas drive a dynamic morphodynamic regime, with  
11        the result that the approach channels to these ports are gradually infilled. Periodic  
12        dredging is therefore necessary to maintain the operativity of the port. A case in point is  
13        Ribadeo (NW Spain), an important port for the economy of the area. In this work, the  
14        sediment transport patterns of the estuary (Ria de Ribadeo) are investigated through  
15        high-resolution numerical modelling and field measurements covering a 4-year period.  
16        On this basis, a decision-aid tool is developed that enables to predict the time evolution  
17        of the approach channel and thus contributes to the planning of dredging operations and,  
18        more generally, the maintenance of adequate operativity levels in a cost-effective way.

19        **Keywords:** estuary; dredging; port; sediment transport; navigation channel; numerical  
20        modelling.

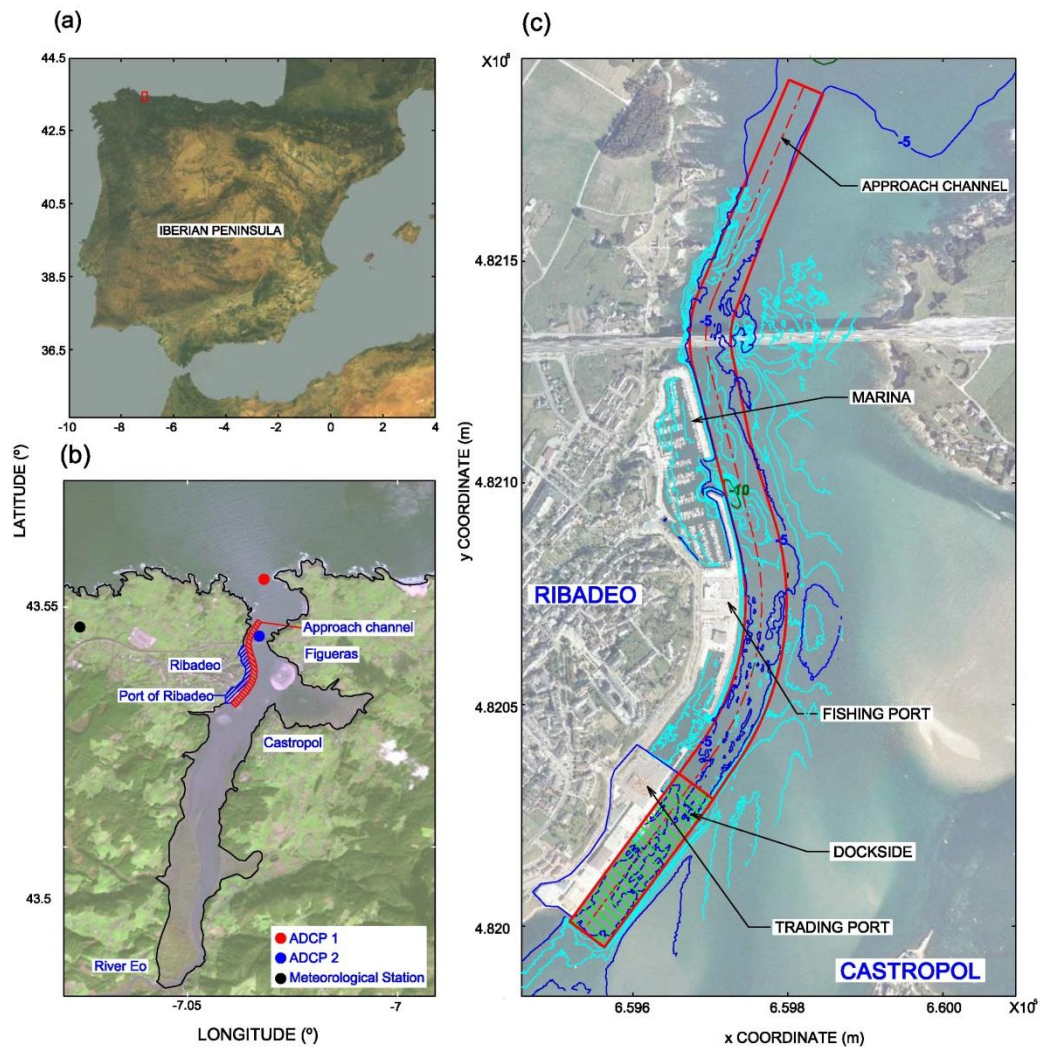
21        \*Corresponding author. Tel.: +34 982 285900; fax: +34 982 285926. E-mail address:  
22        rodrigo.carballo@usc.es (R. Carballo).

23 **1. INTRODUCTION**

24 Shipping may be affected by a number of coastal processes (López and Iglesias, 2013;  
25 López et al., 2015; Teodoro et al., 2014; Rosa-Santos et al., 2009), not least sediment  
26 transport and its repercussions on restricted or semi-restricted navigation channels.  
27 Sediment infilling may affect port operativity by limiting the time for vessels to access,  
28 or depart from, a port. This is the case of a number of ports located in rias in Galicia  
29 (NW Spain).

30 A ria is a particular type of estuary: a drowned river valley in which the accumulation of  
31 sediment since the Holocene transgression has not kept pace with sealevel rise, and  
32 therefore the bathymetry reflects closely the topography of the original river valley.  
33 Galician rias are generally characterised as positive, partially mixed estuaries (Iglesias  
34 et al., 2008).

35 The Port of Ribadeo is located in the middle section of the Ribadeo ria (in the  
36 vernacular, Ria de Ribadeo or Ria del Eo, after the name of the river), at 43° 32.865' N,  
37 007° 02.054' W (**Figure 1**), and is the largest in trade volume of all the ports managed  
38 by the Regional Port Authority (Ports of Galicia). It has a great importance for the local  
39 and regional economy, with a hinterland exceeding a radius of 50 km from the port,  
40 which generates a considerable Short Sea Shipping.



42

43 Figure 1. Location of Ría de Ribadeo (b) and Port of Ribadeo (c) in NW Spain (a).

44 The strong tidal currents in the Ria of Ribadeo (up to  $2 \text{ ms}^{-1}$ ) and the resulting residual  
 45 circulation patterns (Ramos et al., 2013) cause large amounts of sediments to be  
 46 transported, steadily infilling the approach channel to the Port of Ribadeo. A reduction  
 47 in depth in the approach channel means that larger tidal levels are required for ships to  
 48 access the Port, thereby limiting the operativity of the port and, consequently,  
 49 threatening the economic activity in the area (García-Morales et al., 2015). For this  
 50 reason, the port authority undertakes periodic dredging of the approach channel so as to  
 51 maintain operativity.

52 The aim of this work is to define a new integrated approach for the analysis of dredging  
53 operations in shallow coastal areas, such as estuaries, allowing the definition of an  
54 appropriate plan ensuring an adequate operativity at lower maintenance costs. With this  
55 aim, firstly, in Section 2, the requirements of the approach channel to the Port of  
56 Ribadeo are thoroughly defined. Next, in Section 3, high-resolution numerical  
57 simulations based on accurate field measurements are conducted covering a 4-year  
58 period. In Section 4, the tidal levels at the Port of Ribadeo computed through numerical  
59 modelling are analysed. Then, the results obtained in the aforementioned sections are  
60 combined leading to a decision-aid tool for the planning of dredging operations. Finally,  
61 in Section 5 the main conclusions of this work are presented.

62

## 63 **2. REQUIREMENTS OF THE APPROACH CHANNEL**

### 64 ***2.1. Determining factors***

65 A correct definition of the geometry of the approach channel and harbour basin of a port  
66 located in a depth-limited area is of great importance for its appropriate functioning.  
67 The requirements for these areas are calculated in the present work for the Port of  
68 Ribadeo following a comprehensive methodology based on the *Recommendation for*  
69 *Design of Maritime Configuration of Ports, Approach Channels and Harbour Basins*  
70 (Puertos del Estado, 1999b; Álvarez, 2013) .

71 The geometric definition of the navigational channel and harbour basin, both in terms of  
72 cross section and layout, should be based on a thorough knowledge of: i) the area  
73 occupied by the vessel (Sutulo et al., 2010; Briggs et al., 2015), which depends on the  
74 vessel dimensions, ii) the different factors affecting its movements, iii) and the water  
75 level. Furthermore, in the study area it is necessary to consider that the orientation of the

76 approach channel is similar to that of the breakwaters and dock of the Commercial Port  
 77 of Ribadeo (**Figure 1**), and their foundations are at  $-5.00$  m relative to the datum (LAT,  
 78 lowest astronomical tide); therefore, the maximum dredging depth relative to the datum  
 79 should not exceed 5 m to avoid undermining the structures. This is indeed the depth at  
 80 which the approach channel is currently dredged during maintenance operations, and the  
 81 depth retained for the following analysis.

82 In the present study the cross section and layout requirements are defined based on the  
 83 design vessel, i.e. the vessel which best represents the different types of vessels  
 84 operating in the area of interest. With this aim, a comprehensive study of the shipping at  
 85 the Port of Ribadeo was conducted. In total, during 2014 a total of 176 vessels operated  
 86 at this Port, of which 158 were of general cargo, the remaining being composed of nine  
 87 passenger ships, 4 gearless container vessels, 4 research vessels, 3 fishing trawlers and 1  
 88 bulk carrier. After a thorough analysis of the characteristics of the different types of  
 89 vessels, the design vessel at this Port is defined. Its characteristics are shown in **Table 1**.

90 [TABLE 1]

91 Table 1. Characteristics of the design vessel at the Port of Ribadeo

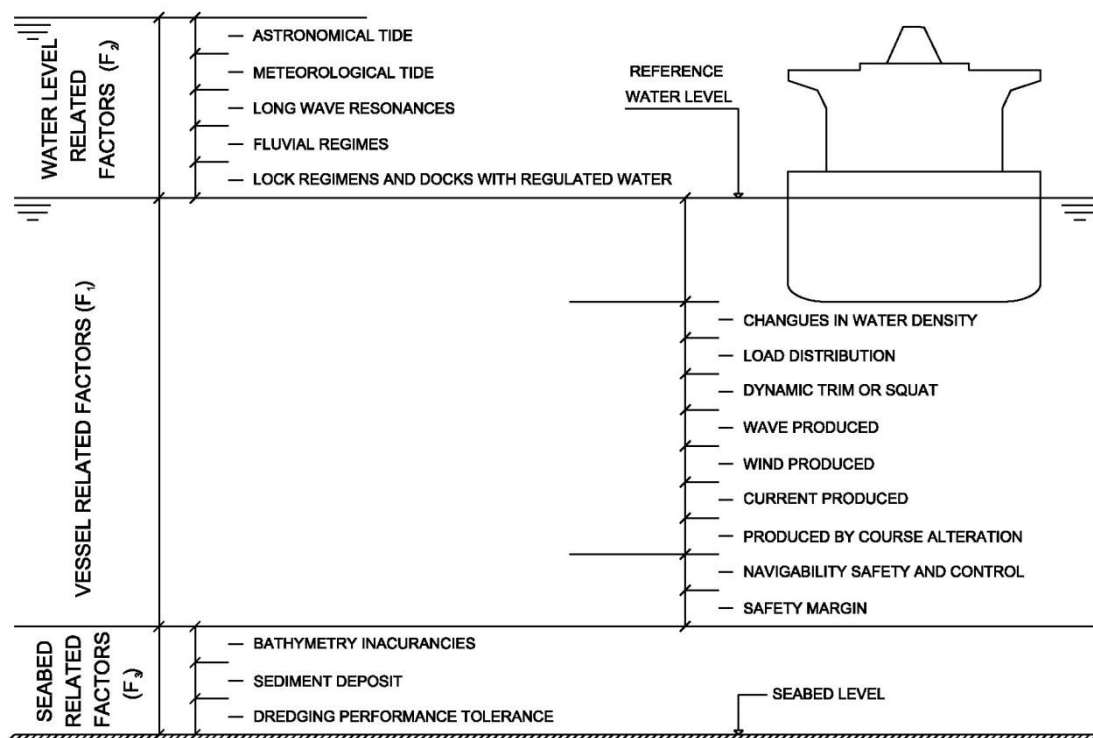
<b>Parameter</b>	<b>Measure</b>
Gross Tonnage	2,700 GT
Length	90 m
Length between perpendiculars	85 m
Draught	5.72 m
Deep load draught	5.41 m
Moment of inertia	11,449 kg m <sup>2</sup>
Freeboard	1.79 m
Depth	7.2 m

92

93 **2.2. Cross-section requirements**

94 The cross section of a channel is sometimes designed in a deterministic way, i.e. on the  
95 basis of a single parameter (i.e. the draught of design vessel); it is more adequate,  
96 however, to take into account a number of factors (Puertos del Estado, 1999a) (**Figure**  
97 **2**).

98 [FIGURE 2]



99

100 Figure 2. Sketch showing the factors considered in the design of the cross section of the  
101 approach channel. [Source ROM 3.1 99 Part VII].

102 The first set of factors, represented by  $F_1$ , integrates all the factors depending on the  
103 vessel itself. It represents the lowest level that any point of the vessel can reach in  
104 relation to the mean level of the water where it is located. For the definition of  $F_1$ , in the  
105 present work a thorough study of the sea conditions in the area is conducted (Álvarez,

106 2013). This information combined with the characteristics of the design vessel allows  
107 the computation of  $F_1$ . The second set of factors, represented by  $F_2$ , provides an analysis  
108 of the tides and other variations in the mean water level (astronomical and  
109 meteorological tides, variations in river flows, etc...), i.e. a factor determining the  
110 reference level of the water where the vessel is located. This is a key factor given that in  
111 the case of a vessel with specific depth requirements (larger than 5 m depth in the  
112 present application), a certain tidal level is required for them to operate in the area.  
113 Finally,  $F_3$  includes the last set of factors depending on the seabed, including  
114 bathymetry inaccuracies, sediment deposits and dredging performance tolerances  
115 (Álvarez, 2013). The values of the different factors considered in the present work are  
116 summarised in **Table 2**.

117

118

119

120

121

122

123

124

125

126

127

[TABLE 2]

128 Table 2. Parameters for prevention of grounding in the channel

<b>PARAMETERS</b>		<b>VALUE (m)</b>
	Static draught	5.41
	Additional draught due to changes in water density	0.16
	Additional draught due to cargo distribution	0.20
Vessel related factors ( $F_1$ )	Dynamic trim or squat	0.62
	Motions caused by waves	0.10
	Heeling caused by wind	0.08
	Clearance for safety control of the vessel's maneuverability	0.5
	<b>Total (<math>F_1</math>)</b>	<b>7.07</b>
Water level related factor ( $F_2$ )	Astronomical tide	Variable
	<b>Total (<math>F_2</math>)</b>	<b><math>F_1+F_3</math>-channel depth</b>
	Margin for bathymetry inaccuracies	0.07
Seabed related factors ( $F_3$ )	Deposit of sediments	Variable (0 after dredging)
	Dredging performance tolerance	0.37
	<b>Total (<math>F_3</math>)</b>	<b>0.37</b>

129

130 The required water depth will be the result of considering both the vessel and seabed  
131 related factors,  $F_1$  and  $F_3$ , respectively. Therefore, a total of 7.44 m is required for the  
132 design vessel to access or leave the Port of Ribadeo. Given that the water depth of the  
133 approach channel for operation purposes at LAT is set to 5 m, the required tidal level or  
134  $F_2$  is 2.44 m.

135

136



137 **2.3. Layout requirements**

138 The layout of the channel has to be adapted to the local morphological aspects, as well  
139 as to technical, economic and environmental constraints. In the case of the Port of  
140 Ribadeo, the approach channel has a total length of 2,262 m in three straight and two  
141 curved stretches. The two curved stretches have a radius,  $r$ , of 260.5 m and 639 m,  
142 respectively. For technical and safety reasons the approach channel to this port consists  
143 of a single lane fairway whose requirements are calculated in the present study for the  
144 design vessel.

145 As a result of the implementation of the aforementioned methodology the overall width  
146 of the fairway is set to 90 m and 100 m in straight sections and curves, respectively.  
147 Finally, due to the presence of moorings lines in the dockside, the straight section in this  
148 area is increased 15 m (Álvarez, 2013). The cross section and layout requirements thus  
149 obtained are shown in **Figure 3** and the resulting plan view of the area occupied by the  
150 approach channel in **Figure 4**.

151

152

153

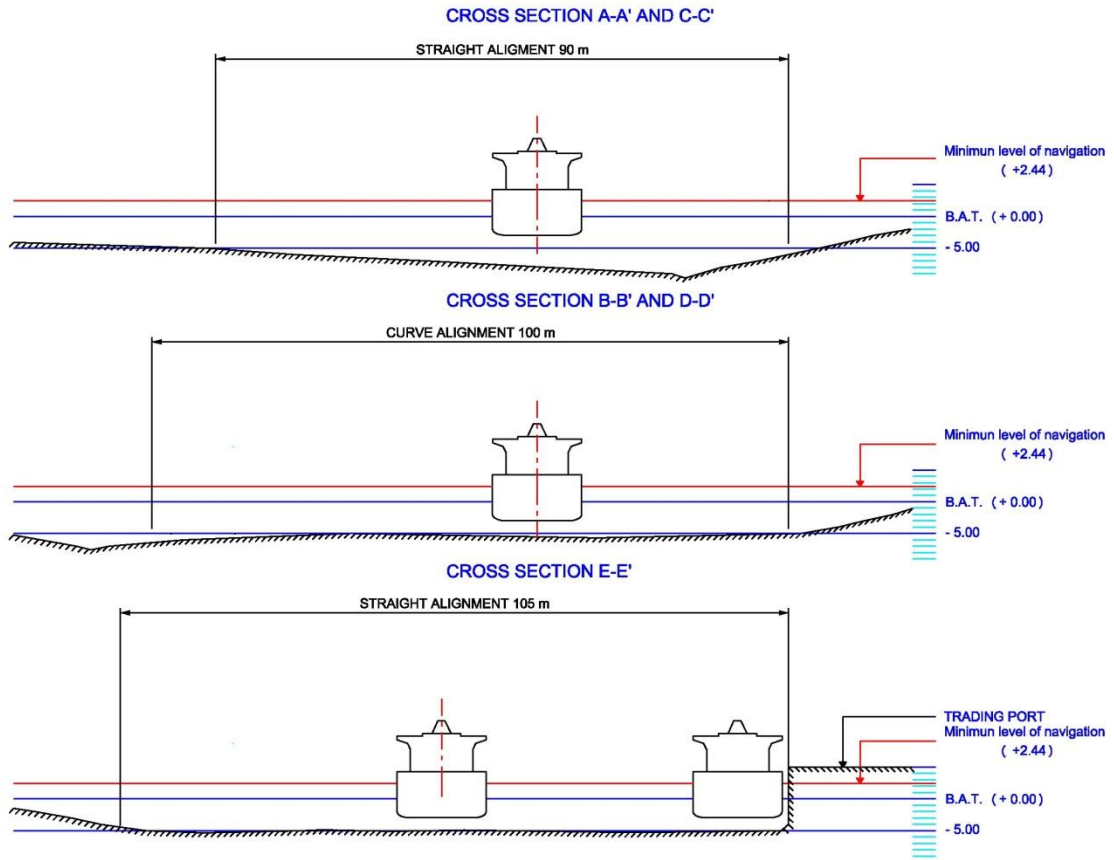
154

155

156

157

158



160

161 Figure 3. Cross section and layout requirements of the approach channel of the Port of

162 Ribadeo.

163

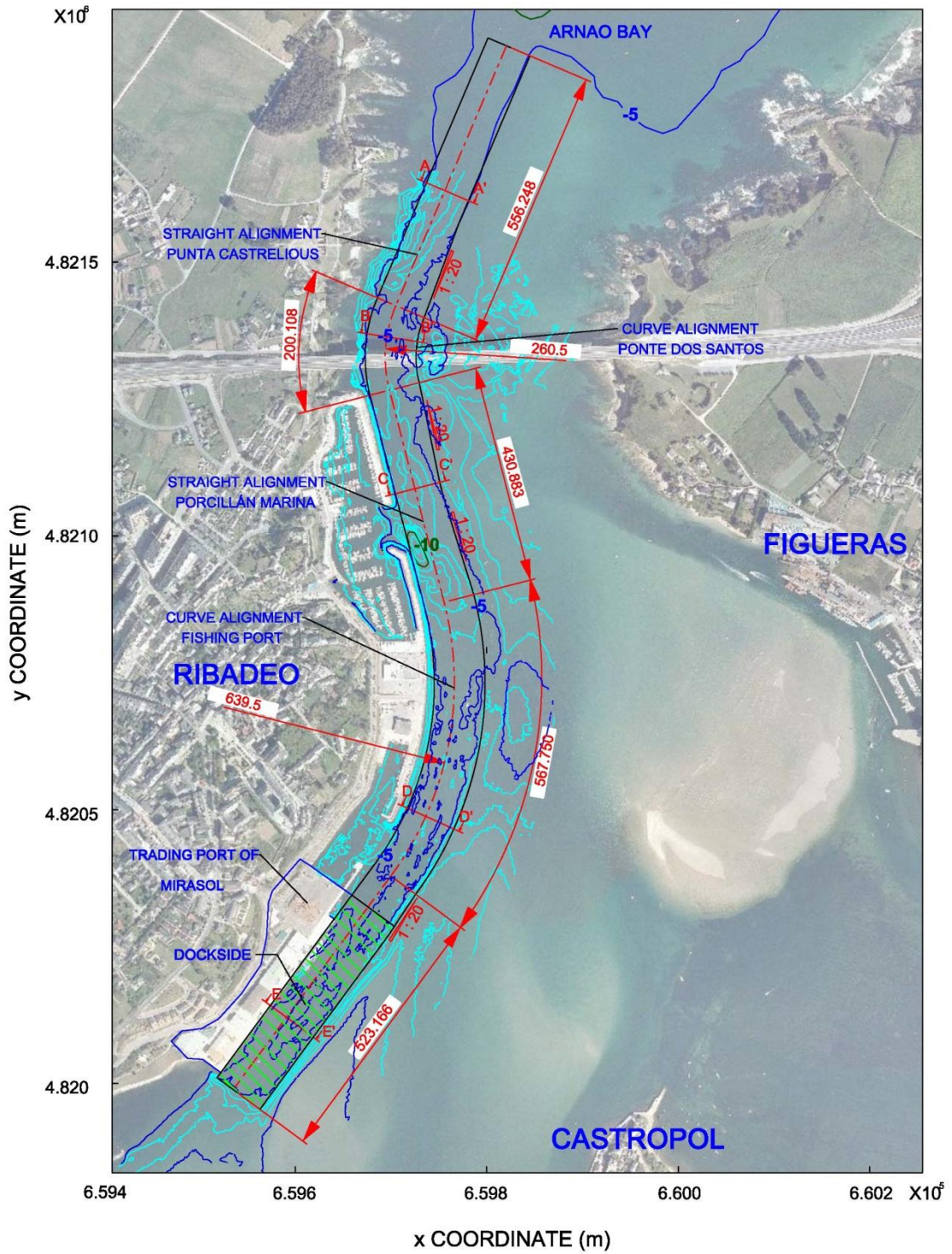
164

165

166

167

168



170

171 Figure 4. Plan view representation of the area occupied by the approach channel.

172

173 **3. NUMERICAL MODEL**

174 **3.1. Model equations**

175 The next step consists in studying the evolution of the bottom of the approach channel  
 176 defined in Section 2 through a 4-year period, accounting for the complex  
 177 morphodynamics of this ria. With this aim a finite-difference Navier-Stokes 3D solver,  
 178 Delft3D, is implemented on the ria, which has been successfully used in other Galician  
 179 Rias [e.g. (Carballo et al., 2009a; Iglesias and Carballo, 2009; Prumm and Iglesias,  
 180 2016; Sanchez et al., 2014; Iglesias et al., 2008; Carballo et al., 2009b; Sánchez et al.,  
 181 2013)]. Delft3D-FLOW is a hydrodynamic and transport model which solves the  
 182 Navier–Stokes equations for an incompressible fluid under the shallow water and  
 183 Boussinesq assumptions. The model equations read:

184 
$$\frac{\partial u}{\partial x} + \frac{\partial v}{\partial y} + \frac{\partial w}{\partial z} = Q, \quad (1)$$

185 
$$\left. \begin{aligned} \frac{Du}{Dt} &= fv - g \frac{\partial \zeta}{\partial x} - \frac{g}{\rho_0} \int_{z=z}^{z'=\zeta} \frac{\partial \rho}{\partial x} dz' + \nu_h \left( \frac{\partial^2 u}{\partial x^2} + \frac{\partial^2 u}{\partial y^2} \right) + \nu_v \left( \frac{\partial^2 u}{\partial z^2} \right) \\ \frac{Dv}{Dt} &= -fu - g \frac{\partial \zeta}{\partial y} - \frac{g}{\rho_0} \int_{z=z}^{z'=\zeta} \frac{\partial \rho}{\partial y} dz' + \nu_h \left( \frac{\partial^2 v}{\partial x^2} + \frac{\partial^2 v}{\partial y^2} \right) + \nu_v \left( \frac{\partial^2 v}{\partial z^2} \right) \end{aligned} \right\}, \quad (2)$$

186 
$$\frac{\partial p}{\partial z} = -\rho g, \quad (3)$$

187 
$$\frac{Dc}{Dt} = D_h \left( \frac{\partial^2 c}{\partial x^2} + \frac{\partial^2 c}{\partial y^2} \right) + D_v \frac{\partial^2 c}{\partial z^2} - \lambda_d c + R. \quad (4)$$

188 where  $u$ ,  $v$  and  $w$  represent the components of the velocity in the directions  $x$ ,  $y$  and  $z$ ,  
 189 respectively;  $Q$  represents the sources of mass per unit area;  $f$  is the Coriolis parameter;  
 190  $g$  is the gravitational acceleration;  $\zeta$  is the free surface elevation relative to  $z = 0$ ;  $\nu_h$  and

191  $v_v$  stand for the horizontal and vertical kinematic eddy viscosity coefficients,  
 192 respectively;  $\rho$  and  $\rho_0$  are the water density and the reference density of sea water,  
 193 respectively;  $c$  represents the mass concentration of any constituent (e.g. salinity and  
 194 temperature);  $D_h$  and  $D_v$  stand for the horizontal and vertical eddy diffusivity  
 195 coefficients, respectively;  $\lambda_d$  represents the first order decay process; finally,  $R$  is the  
 196 source term per unit area.

197 In addition, the model computes sediment transport and morphological updating by  
 198 simulating both bed-load and suspended load transport. In the case of suspended load,  
 199 the advection-diffusion equation (mass balance) is solved, which reads:

$$\begin{aligned}
 & \frac{\partial c^{(l)}}{\partial t} + \frac{\partial uc^{(l)}}{\partial x} + \frac{\partial vc^{(l)}}{\partial y} + \frac{\partial (w - w_s^{(l)})c^{(l)}}{\partial z} \\
 200 & - \frac{\partial}{\partial x} \left( \epsilon_{s,x}^{(l)} \frac{\partial c^{(l)}}{\partial x} \right) - \frac{\partial}{\partial y} \left( \epsilon_{s,y}^{(l)} \frac{\partial c^{(l)}}{\partial y} \right) - \frac{\partial}{\partial z} \left( \epsilon_{s,z}^{(l)} \frac{\partial c^{(l)}}{\partial z} \right) = 0
 \end{aligned} \tag{5}$$

201 where  $c^{(l)}$  is the mass concentration of the sediment fraction ( $l$ );  $\epsilon_{s,x}^{(l)}$ ,  $\epsilon_{s,y}^{(l)}$ ,  $\epsilon_{s,z}^{(l)}$   
 202 stands for eddy diffusivities of the sediment fraction ( $l$ ); finally,  $w_s^{(l)}$  is the sediment  
 203 settling velocity of the sediment fraction ( $l$ ). The local flow velocities and eddy  
 204 diffusivities are computed by the hydrodynamic model. The sediment transport is  
 205 computed in the same way as the transport of any other constituent (e.g. salinity or  
 206 temperature); nevertheless, there exist a number of important differences between  
 207 sediments and other constituents —exchange of sediment between the bed and the flow,  
 208 or parameters such as the settling velocity, whose appropriate computation is of major  
 209 importance for obtaining accurate results (Deltares, 2011).

210 The effect of sediments on fluid density is considered by using the empirical  
 211 relationship formulated by UNESCO (Unesco, 1981) which accounts for the varying  
 212 temperature and salinity. In the case of the sediment transport, this relationship is

213 extended in order to consider the density effect of sediment fractions in the fluid  
 214 mixture. For this purpose the mass of the different sediment fractions is added and the  
 215 displaced water mass subtracted. This can be expressed as:

$$216 \quad \rho_{mix}(S, c^{(l)}) = \rho_w(S) + \sum_{l=1}^{l_{sed}} c^{(l)} \left( 1 - \frac{\rho_w(S)}{\rho_s^{(l)}} \right) \quad (6)$$

217 where  $\rho_w(S)$  is the specific water density with salinity concentration  $S$ ;  $\rho_s^{(l)}$  is the  
 218 specific density of the sediment fraction ( $l$ ); finally  $l_{sed}$  is the number of sediment  
 219 fractions.

220 The settling velocity for non-cohesive and cohesive sediment fractions is computed with  
 221 different formulations. In the case of non-cohesive sediments the Van Rijn method is  
 222 implemented (Van Rijn, 1993), which depends on the diameter of the sediment in  
 223 suspension:

$$224 \quad w_{s,0}^{(l)} = \begin{cases} \frac{(s^{(l)} - 1)gD_s^{(l)2}}{18\nu}, & 65 \mu m < D_s \leq 100 \mu m \\ \frac{10\nu}{D_s} \left( \sqrt{1 + \frac{0.01(s^{(l)} - 1)gD_s^{(l)3}}{\nu^2}} - 1 \right), & 100 \mu m < D_s \leq 1000 \mu m \\ 1.1\sqrt{(s^{(l)} - 1)gD_s^{(l)}}, & 1000 \mu m < D_s \end{cases} \quad (7)$$

225 where  $s^{(l)}$  is the relative density of sediment fraction ( $l$ ) ( $s^{(l)} = \frac{\rho_s^{(l)}}{\rho_w}$ ),  $D_s^{(l)}$  accounts for  
 226 the representative diameter of the sediment fraction ( $l$ ), and  $\nu$  stands for the kinematic  
 227 viscosity coefficient of water.

228 With respect to the cohesive sediment fraction, a complex formulation is used which  
 229 includes the computation of two settling velocities, for fresh water and salt water. For

230 full details about the methodology for modelling this and other processes related to the  
231 cohesive sediment fraction, such as dispersion, erosion or deposition, the reader is  
232 referred to Delft Flow Manual (Deltares, 2011).

### 233 *3.2. Model implementation*

234 In the present study, and following previous works on the hydrodynamics of this ria  
235 (Ramos et al., 2013), the hydrodynamic and sediment transport model is implemented in  
236 its 2D form with a high spatial resolution (Periáñez et al., 2013). Given that the aim of  
237 this research is to conduct an accurate assessment of the morphological evolution of the  
238 approach channel over a 4-year period, the numerical grid (**Figure 5**) covers not only  
239 the area of interest (the middle ria) but the entire estuary (including the inner and outer  
240 ria), whose morphodynamics may affect the bedload sediment transport in the channel.  
241 The resolution within the ria is set to 40 m, with the size of the cells increasing  
242 progressively towards the sea boundary, which is located sufficiently distant that  
243 numerical disturbances do not affect the area of interest.

244

245

246

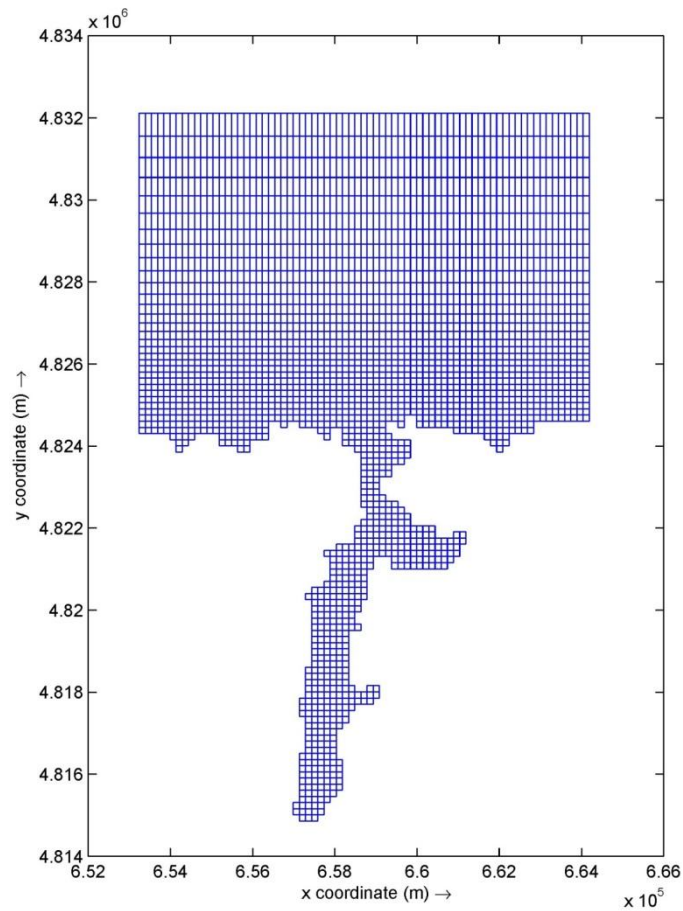
247

248

249

250

251

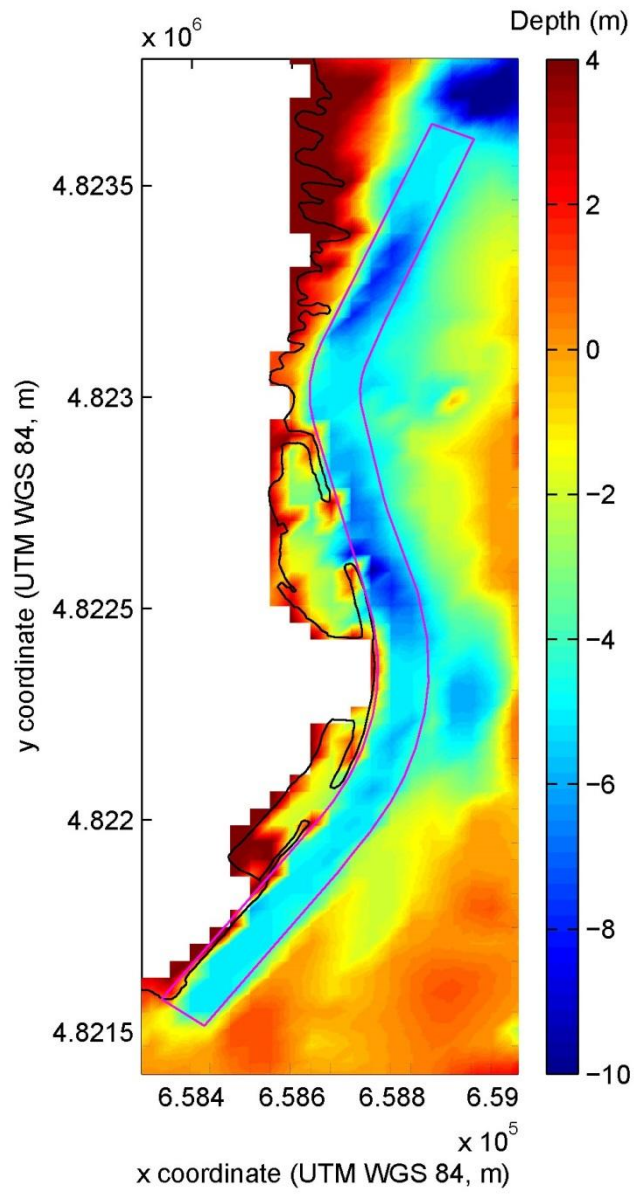


253

254 Figure 5. Numerical grid used for hydro-morphodynamic computations. For clarity only  
 255 1 in 4 grid lines are plotted.

256 The bathymetric data of the ria and the adjoining continental shelf (**Figure 6**) are  
 257 obtained from the relevant nautical charts, which are digitised and interpolated onto the  
 258 computational grid. In addition, the most recent bathymetric data from previous  
 259 dredging operations in the approach channel were also included in the numerical grid.  
 260 Finally, the intertidal areas are modelled by considering topographic data with 5 m of  
 261 resolution. Given that this ria presents large shallow areas, a spatially varying value of  
 262 the Manning coefficient,  $n$ , is input to the model, defined as a function of the water  
 263 depth (**Table 3**) (e.g. Cheng et al., 1993; Dias and Lopes, 2006).





265

266

Figure 6. Bathymetry of the area of study.

267

268

269

270

271

[TABLE 3]

272

Table 3. Manning value,  $n$ , as function of water depth,  $d$ 

$d$ (m)	$n$
$d < -2.0$	0.042
$-2.0 \leq d < -1.5$	0.038
$-1.5 \leq d < -1.0$	0.034
$-1.0 \leq d < -0.5$	0.030
$-0.5 \leq d < 0.0$	0.027
$0.0 \leq d < 0.5$	0.024
$0.5 \leq d < 1.0$	0.022
$1.0 \leq d < 3.0$	0.020
$3.0 \leq d < 10.0$	0.018
$d > 10$	0.015

273

274

275 The turbulent eddy viscosity,  $\nu$ , and diffusivity,  $D$ , are calibration parameters. For the  
276 calibration, field data of water levels and currents measured by an Acoustic Doppler  
277 Profiler (ADCP) (location ADCP 2, **Figure 1**) during three weeks (from 16<sup>th</sup> of October  
278 2011 to 4<sup>th</sup> of November 2011) are compared with model data obtained with different  
279 values of  $\nu$  and  $D$ . The values of the correlation coefficient,  $R$ , for the horizontal  
280 velocities,  $u$  and  $v$  and water levels,  $\eta$ , are presented in **Table 4**. On the basis of these  
281 results, the turbulent eddy viscosity and diffusivity are set to  $5 \text{ m}^2\text{s}^{-1}$ . Then, the  
282 performance of the model using these values is checked at an additional location  
283 (ADCP 1) for the same period (**Table 5**). The good agreement obtained between  
284 simulated and observed values shows that the model is capable of appropriately  
285 capturing the ria hydrodynamics.

286

[TABLE 4]

287 Table 4. Correlation coefficient,  $R$ , between simulated and observed data for different  
 288 eddy viscosities and diffusivities at location ADCP 2.

$\nu, D \text{ (m}^2\text{s}^{-1}\text{)}$	Velocities correlation		Sea level correlation
	$R_U$	$R_V$	$R_\eta$
1	0.8200	0.8912	0.9920
5	0.9449	0.9710	0.9938
15	0.9345	0.9294	0.9920
30	0.9256	0.9277	0.9920
50	0.9024	0.9177	0.9921
100	0.8607	0.8933	0.9920

289

290

291

292

[TABLE 5]

293 Table 5. Correlation coefficient,  $R$ , between simulated and observed data for turbulent  
 294 eddy viscosity and diffusivity set to  $5 \text{ m}^2\text{s}^{-1}$  at locations ADCP 1 and 2.

	$R_U$	$R_V$	$R_\eta$
<i>ADCP 1</i>	0.9451	0.9556	0.9919
<i>ADCP 2</i>	0.9449	0.9710	0.9938

295

296

297

298

299 **3.3. Case study**

300 With the aim of analysing the evolution of the bathymetry of the approach channel  
 301 resulting from the complex morphodynamics of Ria de Ribadeo, the model is run for a  
 302 total of 4 years, from 2012 to 2016. The initial date for the simulations corresponds to  
 303 the date when the last dredging was conducted and therefore accurate depth data of the  
 304 approach channel are available (which in turn is the initial depth considered for  
 305 numerical modelling).

306 All the relevant hydrodynamic and morphodynamic forcing factors are considered in the  
 307 simulation: tide, river discharges, and salinity and temperature at open boundaries, as  
 308 well as the spatial distribution of the sediments. The tide is introduced by considering  
 309 the values of the seven major tidal constituents provided by TPXO data (Egbert et al.,  
 310 1994) (**Table 6**); river discharges are set to the mean historic discharge (April 2009 to  
 311 December 2012) ( $18,83\text{m}^3\text{s}^{-1}$ ); finally, the salinity and temperature at the open  
 312 boundaries are computed through ROMS (Regional Ocean Modelling System) (Otero et  
 313 al., 2008). Regarding the morphological data, the principal model forcing parameters  
 314 considered are shown in **Table 7** (Hu et al., 2009).

315 [TABLE 6]

316 Table 6. Tidal constituents at the ocean boundary of the numerical grid.

Constituent	Amplitude (cm)	Phase (°)
M <sub>2</sub>	125.13	91.40
S <sub>2</sub>	43.96	112.17
N <sub>2</sub>	26.47	71.45
K <sub>2</sub>	12.27	120.23
K <sub>1</sub>	7.14	73.27
O <sub>1</sub>	6.23	324.20
P <sub>1</sub>	2.16	64.82

317

[TABLE 7]

318 Table 7. Principal morphological parameters used in the implementation of the  
319 numerical model.

Parameter	Value
Specific density (Kg/m <sup>3</sup> )	2650
Dry bed density (Kg/m <sup>3</sup> )	1600
Initial sediment layer at bed (m)	5
Median sediment diameter (D <sub>50</sub> )	Spatial distribution

320

321

322 With respect to the grain size, the ria has a complex distribution that must be  
323 characterised if the evolution of the approach channel is to be appropriately modelled  
324 (Flor et al., 1983; Encinar and Rodríguez, 1983; Flor et al., 1992). The spatial  
325 distribution of the mean grain size diameter,  $D_{50}$ , is input to the model following  
326 previous studies, and in particular using measured data (**Figure 7**) provided by the Port  
327 Authority from the latest dredging operations. As a result, the configuration of the  
328 seabed in the channel and the sediment input to the model (**Figure 8**) correspond  
329 exactly with the initial data of the numerical simulation—a prerequisite for ensuring the  
330 accuracy of the model results.

331

332

333

334

335

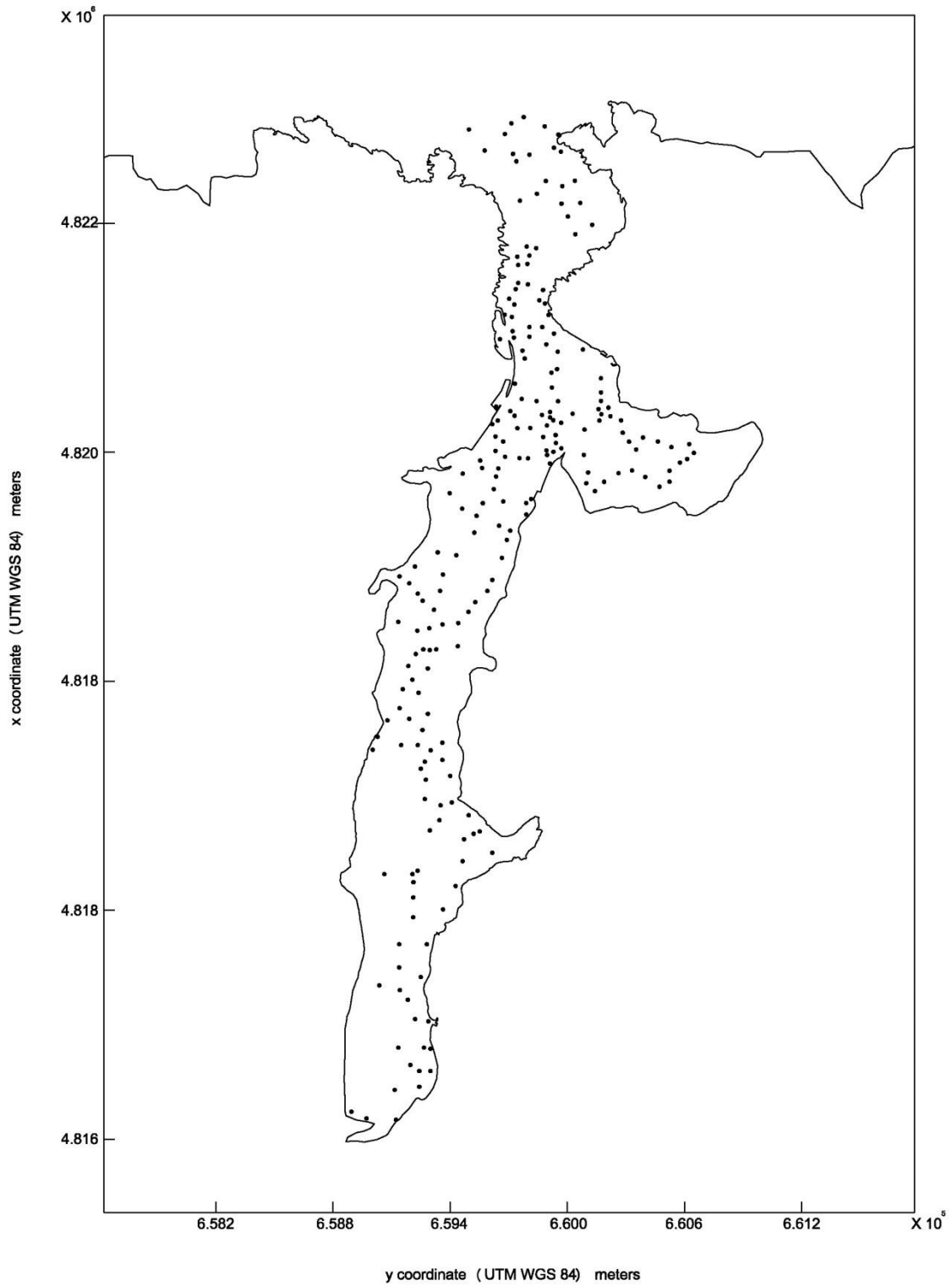
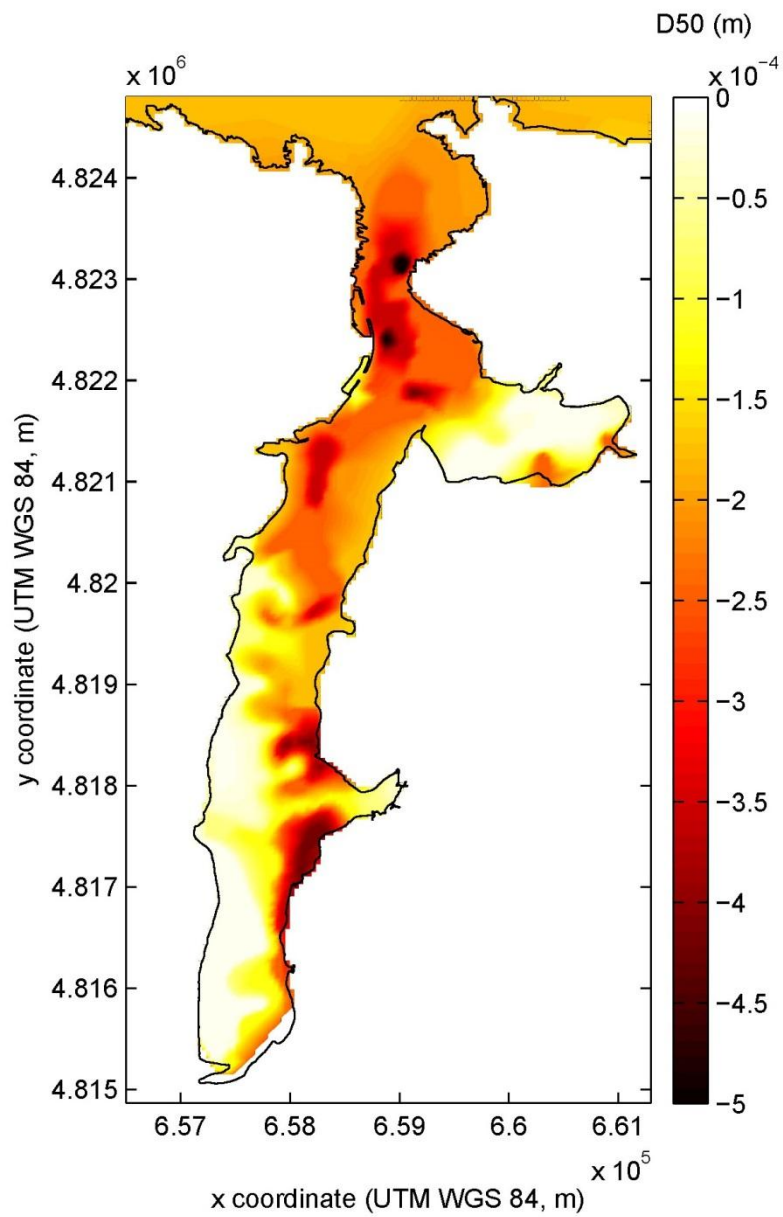


Figure 7.  $D_{50}$  sampling stations.



341

342

Figure 8. Spatial distribution of the mean grain size diameter,  $D_{50}$ .

343

344 The model capability for predicting the evolution of the approach channel is analysed.

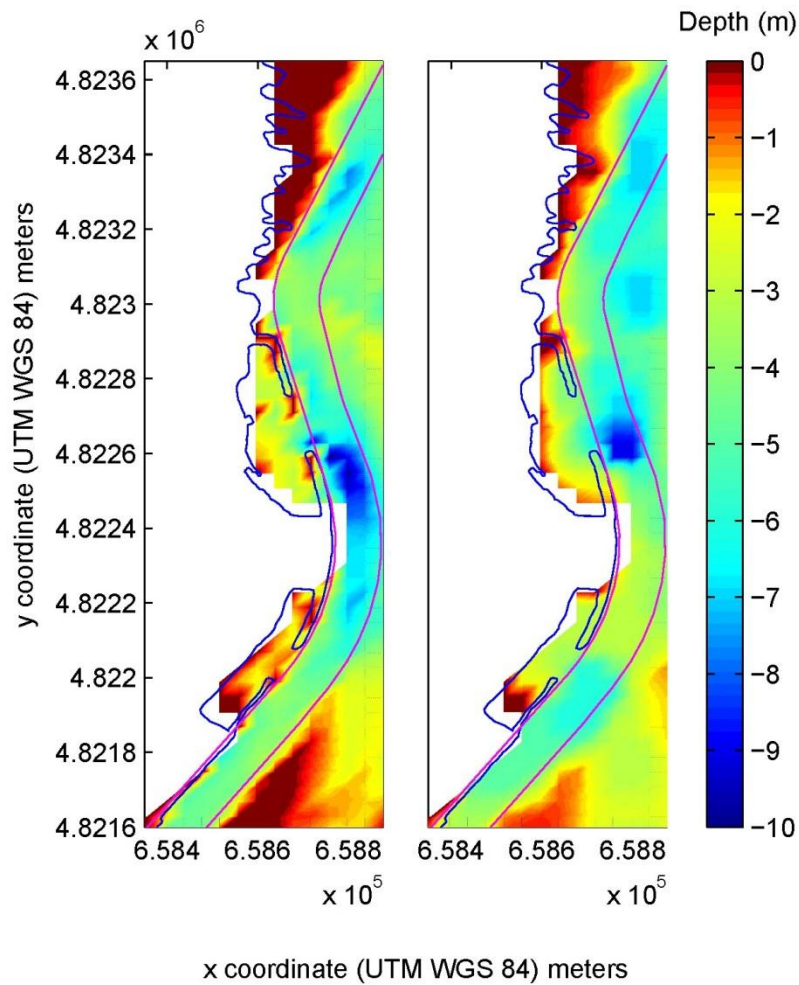
345 For this purpose, the seabed position computed by the model at the end of 4-year period

346 is compared with high-resolution in situ measurements in the area occupied by the

347 approach channel and surroundings gathered at the end of model simulations (year  
348 2016) (**Figure 9**). The correlation coefficient, R, between the bathymetry configuration  
349 predicted by the model (left) and measured (right) is 0.71.

350

[FIGURE 9]



351

352 Figure 9. Bathymetry configuration computed by the model (left) and measured (right)  
353 at the end of model simulations.

354



355 The results obtained prove the ability of the model for accurately reproducing the  
356 bathymetric trends in the approach channel, not least considering the complexity of the  
357 problem.

358

#### 359 **4. HYDROMORPHOLOGICAL RESULTS**

360 The hydrodynamic results obtained through numerical modelling clearly show the  
361 strong currents that occur in the ria, and in particular within the approach channel,  
362 which in part explain the need for frequent dredging discussed in the Introduction. In  
363 **Figure 10** the flow velocities in the middle and outer Ria the Ribadeo are plotted during  
364 mid-flood and mid-ebb of a spring tide (10 March 2012). It can be observed that strong  
365 current velocities occur both during ebb and flood throughout the ria, and in particular  
366 within the approach channel, where velocity magnitudes exceed  $1 \text{ ms}^{-1}$  over large areas,  
367 reaching  $1.5 \text{ ms}^{-1}$  at specific locations. In addition, a tidal asymmetry can be observed,  
368 with larger velocities during flooding. This asymmetry, which has been observed in  
369 other Galician rias (Iglesias and Carballo, 2011; Iglesias and Carballo, 2010), which  
370 may contribute to sediment entrapment in the inner ria and, ultimately, to bedforms such  
371 as megaripples and sand banks.

372

373

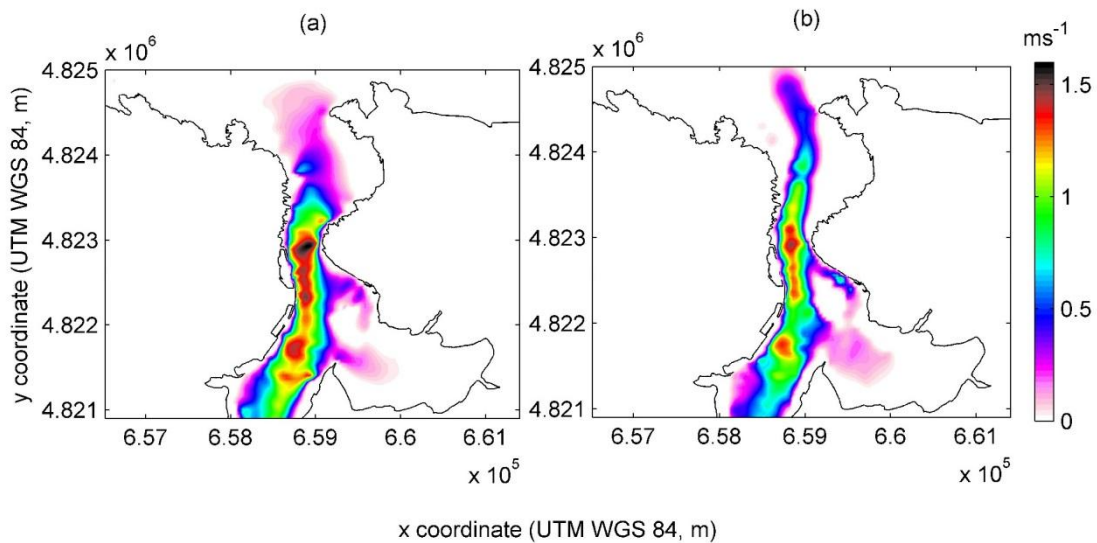
374

375

376

377

[FIGURE 10]



378

379 Figure 10. Mid-flood (a) and mid-ebb (b) depth-averaged flow velocities in the Ría of  
380 Ribadeo.

381

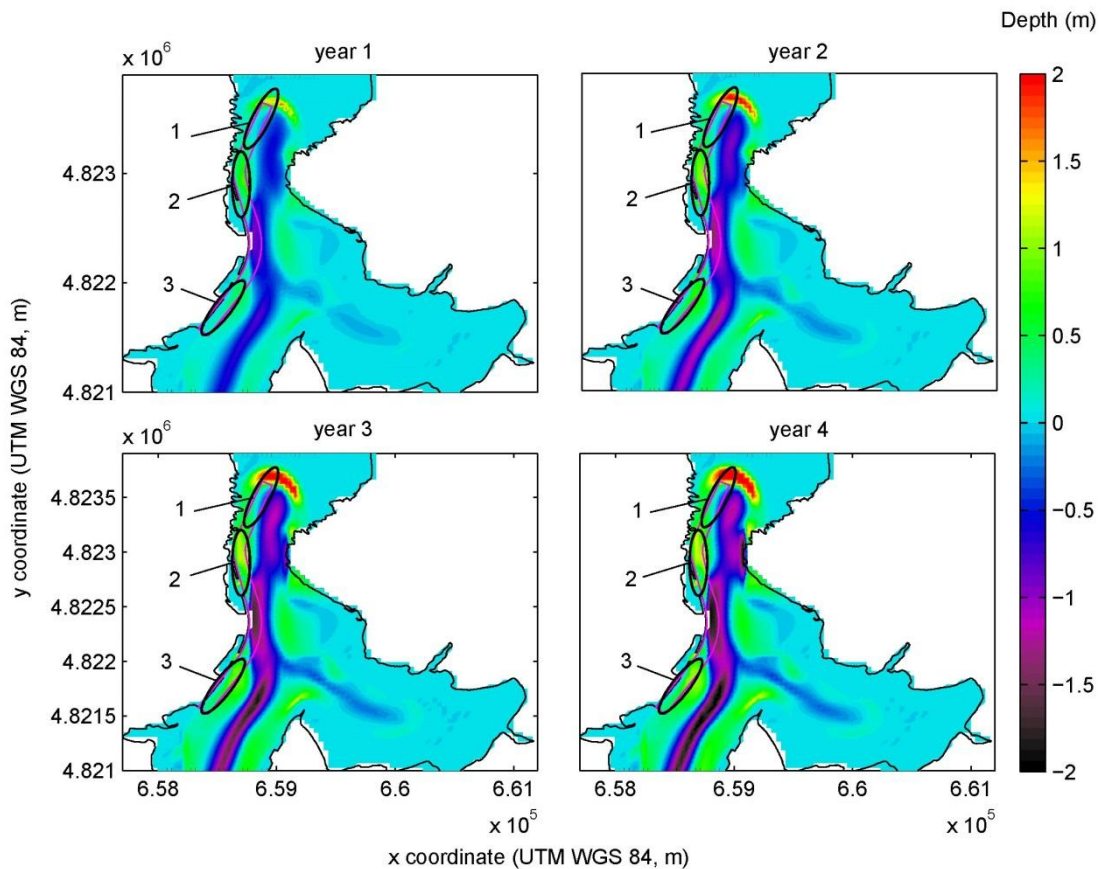
382 These strong currents, as stated, generate an important transport of sediments resulting  
383 in a significant variation of the bed configuration on this coastal area. In **Figure 11** the  
384 evolution of the bed level over a 4-year period is shown. Overall, a relationship can be  
385 observed between current velocities and sediment transport, with accretion associated  
386 with the areas of weaker current velocities and erosion with those boasting stronger  
387 velocities.

388

389

390

391



393

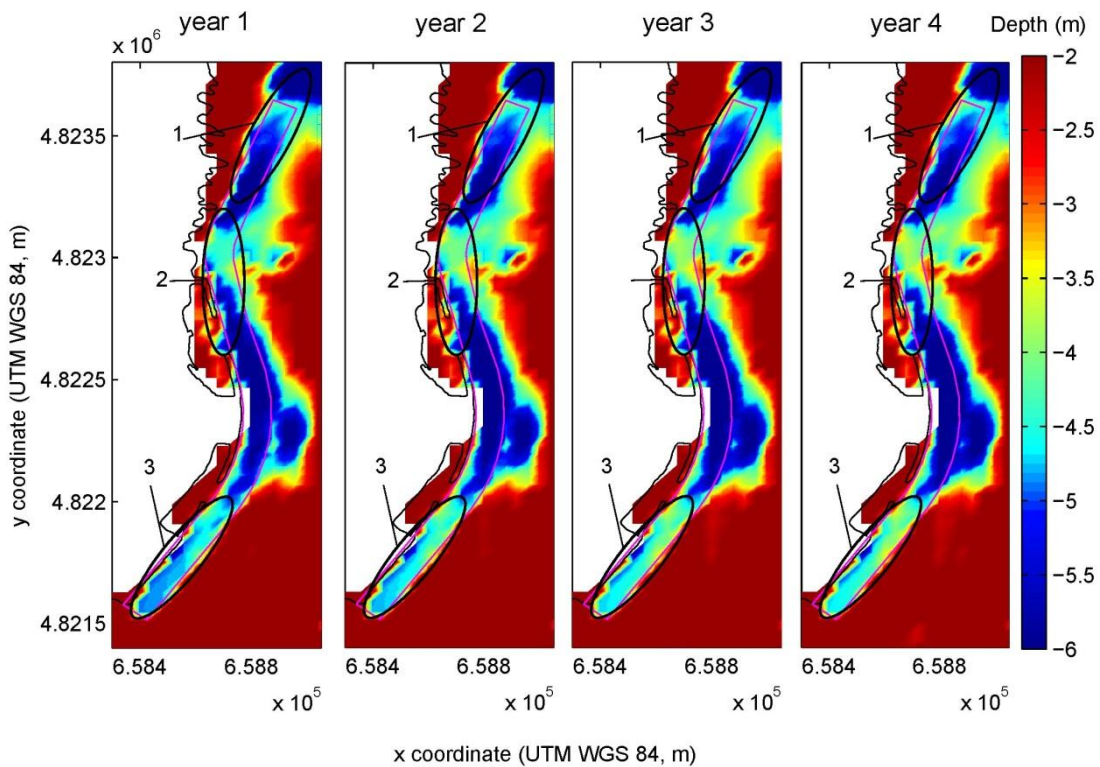
394 Figure 11. Bed update of the Ría de Ribadeo over a 4-year period (the approach channel  
 395 is represented with a red line). Positive and negative values indicate an increase and  
 396 reduction of the bed level, respectively.

397

398 In the case of the approach channel to the Port of Ribadeo defined in Section 2, three  
 399 important accretion areas can be identified: (1) the outer approach channel, with  
 400 accretion of up to 2 m at the end of the 4-year period analysed, (2) the area in front of  
 401 the marina, with an increase in the seabed level of about of 1.5 m, and (3) finally, a  
 402 large area at the end of the channel (dockside), with less than 1 m. Yet, their importance  
 403 for the functioning of the port widely differs stemming from their total depth at the end

404 of the 4-year period analysed, with more than 5 m in the case of the first area (1) and  
405 less than 4-5 m in the second and third areas (2, 3) (**Figure 12**). Within the rest of the  
406 channel (roughly the middle sections, corresponding to the area in front of the fishing  
407 port), significant erosion occurs which naturally does not pose a threat for the  
408 appropriate functioning of the port from a navigational standpoint. Still, this erosion can  
409 lead to scour problems at the breakwater, which was projected for a water depth of 5 m  
410 (LAT) and should be further analysed.

411 [FIGURE 12]



412

413 Figure 12. Evolution of the depth within the approach channel to the Port of Ribadeo  
414 over the a 4-year period.

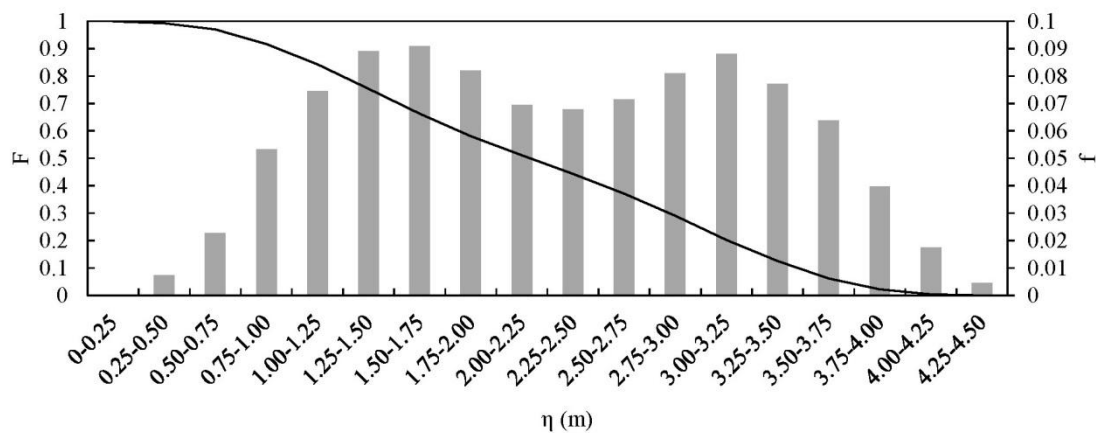
415

416

417 **5. OPERATIVITY AND DREDGING: AN INTEGRATED APPROACH**

418 It has been shown that a total of 7.44 m is necessary for the design vessel to operate at  
 419 the Port of Ribadeo. Therefore, given that the water depth within the approach channel  
 420 cannot exceed 5 m (LAT) for constructive reasons, the required astronomical tidal level  
 421 is 2.44 m (Section 2). On this basis, the operativity can be computed, i.e. the period of  
 422 time during which there is the adequate level for port operation (2.44 m). For this  
 423 purpose, the tidal levels at the Port of Ribadeo are computed in this work by means of  
 424 numerical modelling throughout a complete year, and on that basis their monthly  
 425 discrete frequency,  $f$ , and cumulative frequency,  $F$ , obtained. In **Figure 13** the discrete  
 426 and cumulative frequencies are shown in terms of annual figures for clarity purposes.

427 [FIGURE 13]



428  
 429 Figure 13. Annual discrete,  $f$ , and cumulative frequencies,  $F$ , of tidal level at the Port  
 430 of Ribadeo computed through numerical modelling.

431

432 From the cumulative frequency of tidal levels, an annual figure of operativity of 4,025  
 433 h/year is obtained (operativity after dredging), i.e. the time during which the tidal level

434 exceeds 2.44 m. In addition, based on the results of the monthly cumulative frequencies,  
 435 the monthly operativity can be also computed. The corresponding results are shown in  
 436 **Table 8.** It emerges that the operativity is virtually constant throughout the year  
 437 resulting from the almost negligible intra-annual differences in the water level  
 438 distribution, thereby the dredging planning in the Port of Ribadeo can be determined on  
 439 the basis of annual figures of operativity.

440 [TABLE 8]

441 Table 8. Average monthly operativity (hours) of the Port of Ribadeo

Month	Total hours	Operativity hours
January	744	341.5
February	672	309.5
March	744	342
April	720	331.5
May	744	341.5
June	720	329
July	744	343
August	744	340.5
September	720	331
October	744	342.5
November	720	330.5
December	744	342

442

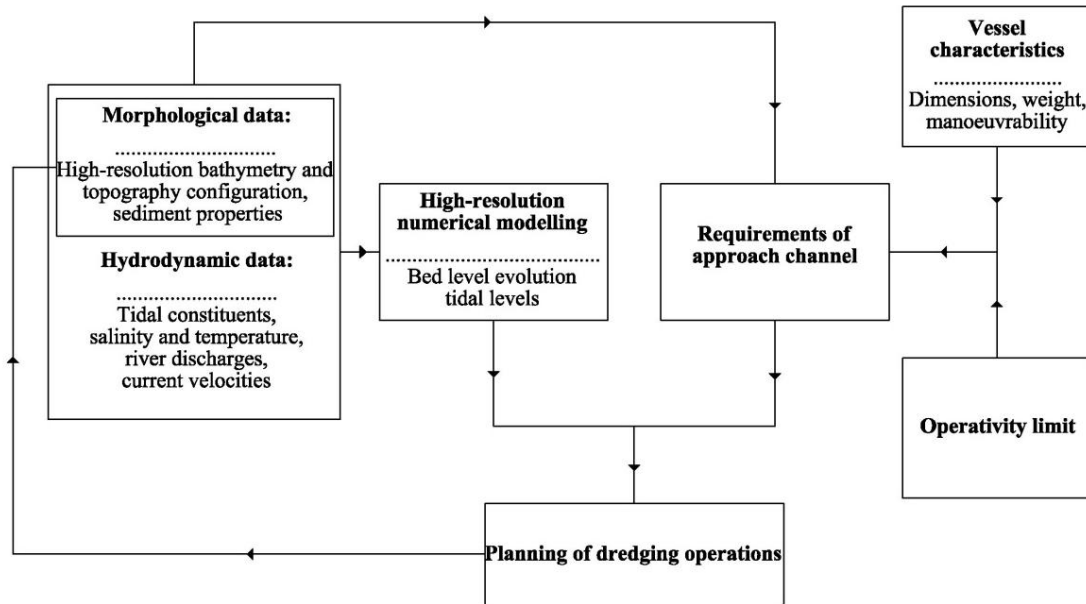
443

444 On the other hand, it has been shown (Section 4) that after dredging there are areas  
445 within the approach channel where the depth is progressively reduced resulting from  
446 sediment transport, which in turn provokes a reduction of the operativity of the port. For  
447 technical and economic reasons, the operativity should never be less than 1,750 h/year,  
448 which corresponds to 20% of the time (Álvarez, 2013). On these grounds, the depth  
449 reduction allowing the minimum operativity level for a design vessel (requiring at least  
450 7.44 m depth) is determined in this work. In the case of considering annual figures —  
451 operativity is virtually constant throughout the year (**Table 8**)— the tidal level available  
452 for the design vessel at the operativity limit (1750 h/year) is 3.29 m (**Figure 13**), which  
453 corresponds with the required level for its operation. In addition, given that the design  
454 vessel requires a total of 7.44 m, the operativity limit occurs when the depth within the  
455 approach channel is reduced to 4.15 m (7.44-3.29 m). This means that the reduction of  
456 water depth resulting from sediment accretion should not exceed 0.85 m in the  
457 considered most restrictive locations —those originally set to 5 m depth after dredging.

458 Now, the 4-year hydro-morphodynamic high-resolution simulations are used so as to  
459 establish both the time point and location within the channel where this depth limitation  
460 (4.15 m) will firstly appear. From the numerical results, this limitation is determined to  
461 occur in first place in the area close to the marina (2) (**Figure 12**) in approximately 3.5  
462 years after dredging. Furthermore, the numerical model results yields the high  
463 resolution bathymetry configuration of the seabed channel at the end of this period;  
464 therefore, the amount of sediments to be dredged so as to rise the operativity to a certain  
465 level can be accurately computed. In the present study if a new dredging is to be  
466 planned at the time point when the operativity limit is reached, a total of 145,760 m<sup>3</sup>  
467 should be dredged for restoring the initial level of operativity established at 4,025  
468 h/year.

469 Given the complexity of the method developed, a flowchart containing the whole  
 470 procedure presented in this work and implemented in the Ria de Ribadeo is shown in  
 471 **Figure 14.**

472 [FIGURE 14]



473

474 Figure 14. Flowchart of the decision-aid tool.

475

476 **6. CONCLUSIONS**

477 The Port of Ribadeo is the largest by trade volume of the ports managed by Ports of  
 478 Galicia Regional Authority. Owing to great importance for the region, a well-defined  
 479 plan for maintaining adequate levels of operativity is fundamental for it to continue  
 480 being a mainstay of the economic activity of the area. The complex morphodynamics of  
 481 the ria, characterised by intense sediment transport, has been shown to affect the  
 482 approach channel, posing a threat to the operativity of the port. With this in view, in the  
 483 present work an integrated approach for defining accurate dredging operation plans was



484 developed and implemented to this coastal area. Based on a state-of-the-art numerical  
485 model, calibrated and validated with field measurements, together with accurate data of  
486 navigational requirements and tidal levels in the area, the implementation of this method  
487 provides the necessary information for conducting cost-effective dredging operations.

488 For this purpose, in the first place the dimensions of the approach channel to the Port of  
489 Ribadeo are accurately defined on the basis of a thorough analysis of the vessels  
490 operating in the area —a total width ranging from 90 m to 105 m depending on the  
491 section considered, and a minimum water depth of 7.44 m. Given that the maximum  
492 depth of the approach channel could not exceed 5 m at some locations (roughly the area  
493 close to the trading port) so as to avoid undermining problems, a tidal level of 2.44 is  
494 necessary for the design vessel to operate in the area. Then, high resolution hydro-  
495 morphodynamic computations are conducted with the aim of characterizing the time  
496 evolution of the bed configuration of the approach channel during a 4-year period  
497 (starting at the last dredging operation). The numerical results clearly show three areas  
498 of significant accretion (approx. 1-2 m at the end of the 4-year period analysed) but only  
499 two of them are critical for the appropriate functioning of the Port —roughly the areas  
500 located in front of the marina and the dockside.

501 The next step of the procedure consists in analysing the tidal level distribution so as to  
502 define the required level for maintaining the minimum operativity, which is established  
503 at 1,750 h/year. This analysis is conducted by determining the monthly and annual  
504 frequencies of the tidal levels at the Port of Ribadeo which are computed in the present  
505 work through numerical modelling. From the results obtained it emerges that a tidal  
506 level of 3.29 m is required for achieving the operativity limit, i.e. the water depth within  
507 the approach channel should not be less than 4.15 m.

508 Finally, the integration of the resulting information allows the determination of the time  
509 point for conducting cost-effective dredging operations. It is found that the minimum  
510 water depth (4.15 m) is firstly achieved in the area close to the marina, approximately  
511 3.5 years after the previous dredging. Furthermore, the present procedure also provides  
512 a detailed bathymetric configuration of the channel and therefore the accurate  
513 computation of the volume to be dredged for increasing the operativity up to a certain  
514 level. In the case of the Port of Ribadeo, should the initial level of operativity is to be  
515 restored (4,025 h/year corresponding to the period during which at least a tidal level of  
516 2.44 m is available), a total of 145,760 m<sup>3</sup> would have to be dredged.

517 In sum, the proposed integrated approach herein presented can contribute to an  
518 appropriate decision making for the planning of dredging operations in shallow water  
519 areas such as estuaries. The procedure was illustrated through the case study of the Port  
520 of Ribadeo, but it could be implemented elsewhere.

521

## 522 **Acknowledgments**

523 The authors are grateful to the Regional Authority Portos de Galicia and Germán Flor  
524 for their essential contribution providing historical morphodynamic data of the Ria de  
525 Ribadeo. During this work Miguel Álvarez has been supported by the I2C (Plan Galego  
526 de Investigación Innovación e Crecemento 2011–2015) of the Xunta de Galicia.

527

528

529

530 **References**

- 531 Álvarez, M., 2013. Morphodynamic Analysis of the Ria De Ribadeo and its Influence  
532 on the Shipping Operations. (in Galician). Universidad de Santiago de Compostela.
- 533 Briggs, M.J., Kopp, P.J., Silver, A.L., Wiggins, W., 2015. Probabilistic model for  
534 predicting deep-draught channel design: Savannah, GA entrance channel. *Ocean Eng.*  
535 108, 276-286.
- 536 Carballo, R., Iglesias, G., Castro, A., 2009a. Numerical model evaluation of tidal stream  
537 energy resources in the Ría de Muros (NW Spain). *Renewable Energy* 34, 1517-1524.
- 538 Carballo, R., Iglesias, G., Castro, A., 2009b. Residual circulation in the Ría de Muros  
539 (NW Spain): A 3D numerical model study. *Journal of Marine Systems* 75, 130.
- 540 Cheng, R.T., Casulli, V., Gartner, J.W., 1993. Tidal, Residual, Intertidal Mudflat  
541 (TRIM) Model and its Applications to San Francisco Bay, California. *Estuarine, Coastal  
542 and Shelf Science* 36, 235-280.
- 543 Deltares, 2011. User Manual Delft3D-FLOW.Simulation of Multi-Dimensional  
544 Hydrodynamic Ows and Transport Phenomena, Including Sediments., Deltares ed,  
545 Delft, The Netherlands.
- 546 Dias, J.M., Lopes, J.F., 2006. Implementation and assessment of hydrodynamic, salt and  
547 heat transport models: The case of Ria de Aveiro Lagoon (Portugal). *Environmental  
548 Modelling and Software* 21, 1-15.

549 Dias, J.M., Sousa, M.C., Bertin, X., Fortunato, A.B., Oliveira, A., Numerical modeling  
550 of the impact of the Ancão Inlet relocation (Ria Formosa, Portugal). *Environmental*  
551 *Modelling & Software* In Press, Corrected Proof.

552 Egbert, G.D., Bennett, A.F., Foreman, M.G.G., 1994. Topex/Poseidon tides estimated  
553 using a global inverse model. *Journal of Geophysical Research* 99, 24821-52.

554 Encinar, M., Rodríguez, G.F., 1983. Aportaciones Para El Conocimiento De La  
555 Dinámica Y Sedimentación De La Ria Del Eo (Asturias-Galicia, NW De España).  
556 Consejería de Agricultura y Pesca del Principado de Asturias.

557 Flor, G., Fernández-Pérez, L.A., Cabrera-Cenal, R., 1992. Características dinámicas y  
558 sus relaciones sedimentarias en la Ria del Eo (Galicia-Asturias, Noroeste de España).  
559 *Revista de la Sociedad Geológica Española* 5, 7-25.

560 Flor, G., Pérez, L.F., Ceñal, R.C., 1983. Aspectos morfológicos del estuario del Eo.  
561 *Trabajos de Geología* 19, 75-97.

562 García-Morales, R.M., Baquerizo, A., Losada, M.Á, 2015. Port management and  
563 multiple-criteria decision making under uncertainty. *Ocean Eng.* 104, 31-39.

564 Hu, K., Ding, P., Wang, Z., Yang, S., 2009. A 2D/3D hydrodynamic and sediment  
565 transport model for the Yangtze Estuary, China. *J. Mar. Syst.* 77, 114-136.

566 Iglesias, G., Carballo, R., 2011. Can the seasonality of a small river affect a large tide-  
567 dominated estuary? The case of the Ria de Viveiro, Spain. *Journal of Coastal Research*  
568 27, 1170-1182.

569 Iglesias, G., Carballo, R., 2010. Effects of high winds on the circulation of the using a  
570 mixed open boundary condition: the Ría de Muros, Spain. *Environmental Modelling &*  
571 *Software* 25, 455-466.

572 Iglesias, G., Carballo, R., 2009. Seasonality of the circulation in the Ría de Muros (NW  
573 Spain). *J. Mar. Syst.* 78, 94-108.

574 Iglesias, G., Carballo, R., Castro, A., 2008. Baroclinic modelling and analysis of tide-  
575 and wind-induced circulation in the Ría de Muros (NW Spain). *Journal of Marine*  
576 *Systems* 74, 475-484.

577 López, I., López, M., Iglesias, G., 2015. Artificial neural networks applied to port  
578 operability assessment. *Ocean Eng.* 109, 298-308.

579 López, M., Iglesias, G., 2013. Artificial Intelligence for estimating infragravity energy  
580 in a harbour. *Ocean Eng.* 57, 56-63.

581 Otero, P., Ruiz-Villarreal, M., Peliz, A., 2008. Variability of river plumes off Northwest  
582 Iberia in response to wind events. *Journal of Marine Systems* 72, 238-255.

583 Perriñez, R., Casas-Ruiz, M., Bolívar, J., 2013. Tidal circulation, sediment and  
584 pollutant transport in Cádiz Bay (SW Spain): A modelling study. *Ocean Eng.* 69, 60-  
585 69. Prumm, M., Iglesias, G., 2016. Impacts of port development on estuarine  
586 morphodynamics: Ribadeo (Spain). *Ocean Coast. Manage.* 130, 58-72.

587 Puertos del Estado, 1999a. Part 7: Cross section requirements, in *Puertos del Estado*  
588 (Ed.), *Recommendations for Maritime Works (Spain) ROM 3.1-99: Designing*  
589 *Maritime Configuration of Ports.*

590 Puertos del Estado, 1999b. Recommendations for Maritime Works (Spain) ROM 3.1-  
591 99: Designing Maritime Configuration of Ports.

592 Ramos, V., Carballo, R., Álvarez, M., Sánchez, M., Iglesias, G., 2013. Assessment of  
593 the impacts of tidal stream energy through high-resolution numerical modeling. Energy  
594 61, 541-554.

595 Rosa-Santos, P., Veloso-Gomes, F., Taveira-Pinto, F., Silva, R., Pais-Barbosa, J., 2009.  
596 Evolution of coastal works in Portugal and their interference with local  
597 morphodynamics. J. Coast. Res., 757-761.

598 Sánchez, M., Iglesias, G., Carballo, R., Fraguera, J.A., 2013. Power peaks against  
599 installed capacity in tidal stream energy. IET Renewable Power Generation 7, 246-253.

600 Sanchez, M., Carballo, R., Ramos, V., Iglesias, G., 2014. Floating vs. bottom-fixed  
601 turbines for tidal stream energy: A comparative impact assessment. Energy 72, 691-701.

602 Sutulo, S., Rodrigues, J., Soares, C.G., 2010. Hydrodynamic characteristics of ship  
603 sections in shallow water with complex bottom geometry. Ocean Eng. 37, 947-958.

604 Teodoro, A., Taveira-Pinto, F., Santos, I., 2014. Morphological and statistical analysis  
605 of the impact of breakwaters under construction on a sand spit area (Douro River  
606 estuary). Journal of Coastal Conservation 18, 177-191.

607 Unesco, 1981. Background Papers and Supporting Data on the Practical Salinity Scale  
608 1978-Unesco.

609 Van Rijn, L.C., 1993. Principles of Sediment Transport in Rivers, Estuaries and Coastal  
610 Seas. Aqua publications Amsterdam.